## Supplementary information:

# Quantum dots encapsulated within phospholipid membranes: phase-dependent structure, photostability, and site-selective functionalization

*Weiwei Zheng, Yang Liu, Ana West, Erin Schuler, Kevin Yehl, R. Brian Dyer, James T. Kindt, Khalid Salaita**

Department of Chemistry, Emory University, Atlanta, Georgia, USA, 30322.

Email: k.salaita@emory.edu

**Supplementary Information List:**

## 1. Synthesis and characterization of CdSe quantum dots (QDs).

**1.1 Materials.** Cadmium oxide (CdO, 99.99%), selenium powder (Se, 99.5%, 100 mesh), tributylphosphine (TBP, 97%), 1-octadecene (ODE), and oleic acid (OA, 90%), were purchased from Sigma Aldrich and used without further purification. A 1.0 M Se stock solution was prepared by adding 157.92 mg Se (2 mmol) in 0.472 g TBP and further diluted with 1.37 g ODE.[1]

**1.2 Synthesis of OA passivated CdSe QDs.** The CdSe QDs were synthesized following a modified literature method.[1,2] In a typical procedure, 0.5 mL OA, 8 mL ODE, and 51.2 mg CdO (0.4 mmol) were loaded in a 25 mL three-neck flask equipped with a stir bar, and the flask was sealed and purged with nitrogen before the temperature was raised to 280 ºC. When the solution turned clear, 2.3 mL of a 1.0 M Se stock solution in TBP and ODE was quickly injected into the reaction to commence nucleation and growth of the nanocrystals. The growth temperature was set to 250 ºC and the reaction mixture was quickly cooled down to room temperature when a desired size was obtained. The synthesized QDs were extracted 3 times with hexane/methanol solution. Finally, the QDs in hexane solution were precipitated out by adding acetone and redissolved in chloroform. The CdSe QDs have the first exitonic peak at 547 nm and an emission peak maximum at 565 nm. The mean nanoparticle diameter and molar concentration were determined from the position and intensity of the first excitonic absorption peak[3] and confirmed with transmission electron microscopy (TEM).

**1.3 Transmission electron microscopy (TEM) and negative staining TEM.** TEM measurements were acquired on a Hitachi H-7500 transmission electron microscope at an accelerating voltage of 75 kV. The L-QD vesicles were visualized by negative staining TEM. Lipids have poor contrast in conventional TEM due to their low electron density. Therefore, negative staining was used to enhance the contrast and identify the lipid vesicles. Specimens were prepared in milli-Q water. The samples were deposited onto glow discharged 200 mesh carbon coated copper grids (Electron Microscopy Sciences). After a ~10 min incubation period, excess liquid was wicked away and specimens were stained with 1% methylamine tungstate (Ted Pella, Inc). Excess stain was wicked away after incubation on the grid for 1 minute. The sample grids were subsequently dried under vacuum.

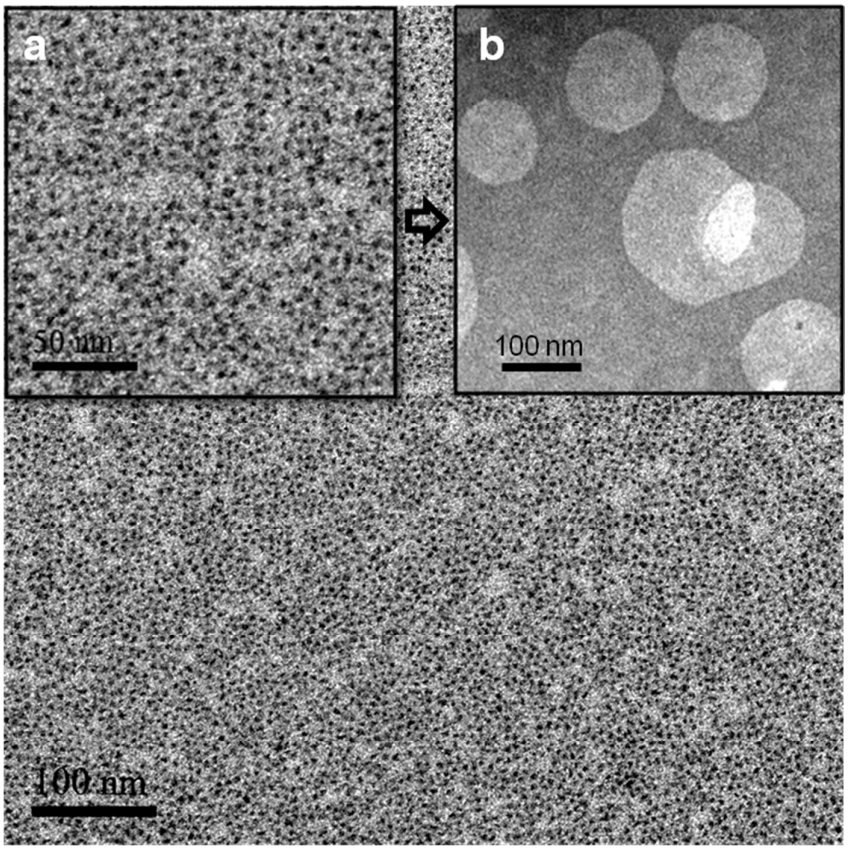


**Figure S1.** TEM images of OA capped 3 nm CdSe QDs. A higher magnification TEM image of the CdSe QDs is shown in inset **(a)**. Inset figure **(b)** is a negative stain TEM image for DSPC-CdSe vesicles.

## 2. Preparation of Lipid-QD (L-QD) vesicles and dynamic light scattering (DLS) measurements.

**2.1 Structure and melting temperature ($T_m$) of lipids.** The lipids used in this study are 1,2-dioleoyl-sn-glycero-3-phosphocholine (DOPC), 1,2-dimyristoyl-sn-glycero-3-phosphocholine (DMPC), 1,2-distearoyl-sn-glycero-3-phosphocholine (DSPC), 1,2-dipalmitoyl-sn-glycero-3-phosphocholine (DPPC), and 1-oleoyl-2-{6-[(7-nitro-2-1,3-benzoxadiazol-4-yl)amino]hexanoyl}-*sn*-glycero-3-phosphocholine (NBD-PC) were purchased from Avanti and used without further purification.

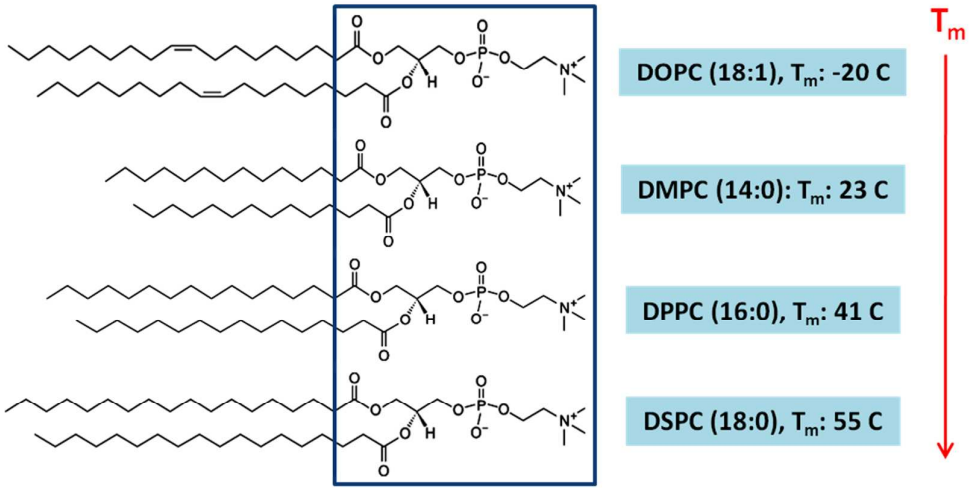


**Figure S2**. Structure and melting temperature ($T_m$) of lipids used to form L-QD vesicles.

**2.2 Preparation of L-QD vesicles.** Small unilamellar vesicles (~170 nm diameter) of the different lipid compositions were prepared by hydration of dried lipid-CdSe film followed by probe sonication. Four different lipids (DOPC, DMPC, DPPC, and DSPC) with melting temperature ($T_m$) from – 20 ºC to 55 ºC were used to generate L-QD vesicles. Lipids and CdSe QDs were mixed in a 5000:1 molar ratio in chloroform for all L-QD vesicle samples. Typically, chloroform solutions of lipid (2.54 µmol) and CdSe QDs (0.5 nmol) were mixed in a 10 mL glass vial and dried under a vacuum using a R-210 rotavapor. The dried film was then hydrated in 1 mL milli-Q $H_2O$. The obtained multilamellar vesicles (MLV) were further sonicated for 1 min using a probe sonicator to generate small unilamellar vesicles (SUV). The amplitude of the sonicator is fixed at 30%. The size of the obtained SUV was checked by dynamic light scattering (DLS) measurements and confirmed with negative stain TEM.

**2.3 Dynamic light scattering (DLS) measurements for lipid vesicles and corresponding L-QD vesicles.**

**Table S1**. Dynamic light scattering data for L-QD vesicles.

| Vesicles | Eff. Diam. (nm)*[1] | Polydispersity*[2] | Sample Quality*[3] |
|---|---|---|---|
| **DOPC** | 183.9 | 0.288 | 9.8 |
| **DOPC-CdSe** | 159.5 | 0.332 | 9.6 |
| **DMPC** | 172.0 | 0.314 | 9.3 |
| **DMPC-CdSe** | 193.0 | 0.290 | 9.7 |
| **DSPC** | 169.4 | 0.326 | 9.5 |
| **DSPC-CdSe** | 171.0 | 0.304 | 9.7 |

*1. Eff. Diam. (Effective diameter) represents an average size of the particles in the sample.

*2. Polydispersity is a measure of non-uniformity that exists in the particles size distribution.

*3. Sample quality is an indication of the difference between the measured and calculated baselines of the correlation function. The highest number (best quality) is 10.

## 3. Optical spectroscopy and optical microscopy.

**3.1 Optical spectroscopy:** UV−visible absorption spectra were recorded using a nanodrop spectrophotometer. The fluorescence of the samples was monitored using a Horiba FluoroMax-3 fluorometer.

**3.2 Optical microscopy:** L-QD vesicles were imaged in aqueous solution at room temperature. The microscope was Nikon Eclipse Ti driven by the Elements software package. The microscope features an Evolve electron multiplying charge coupled device (CCD; Photometrics), an Intensilight epifluorescence source (Nikon), a CFI Apo 100× (numerical aperture (NA) 1.49) objective (Nikon) and a TIRF launcher with two laser lines: 488 nm (10 mW) and 638 nm (20 mW). This microscope also includes the Nikon Perfect Focus System, an interferometry-based focus lock that allowed the capture of multipoint and time-lapse images without loss of focus. The microscope was equipped with the following Chroma filter cubes: TIRF 488, TIRF 640, FITC and reflection interference contrast microscopy (RICM).

To characterize the L-QD hybrid vesicles structure obtained in the study, we monitored the emission of both CdSe QDs and fluorescent 1-oleoyl-2-{6-[(7-nitro-2-1,3-benzoxadiazol-4-yl)amino]hexanoyl}-*sn*-glycero-3-phosphocholine (NBD-PC) lipids doped in the lipid vesicles. The colocalization of CdSe QDs and NBD-PC in DSPC (Figure 1E-G and Supporting Figure S3) and DOPC (Supporting Figure S4) vesicles indicates the successful incorporation of QDs in the lipid membrane.

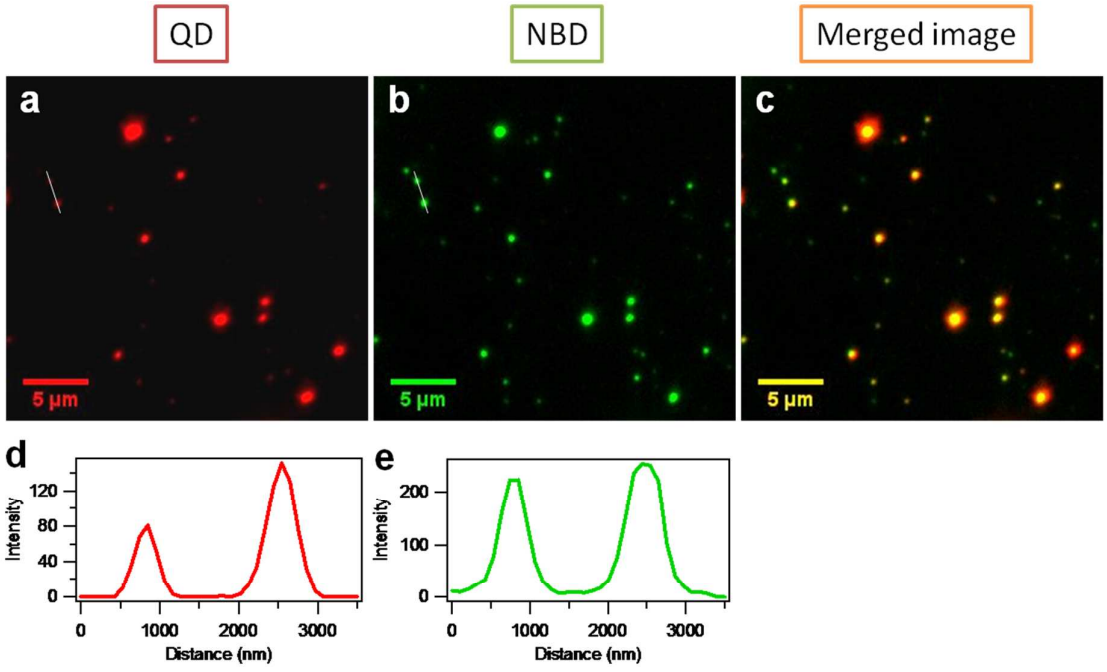


**Figure S3.** Colocalization of CdSe QDs and NBD doped DOPC vesicles.

**4. Temperature-Dependent FTIR Spectroscopy.**

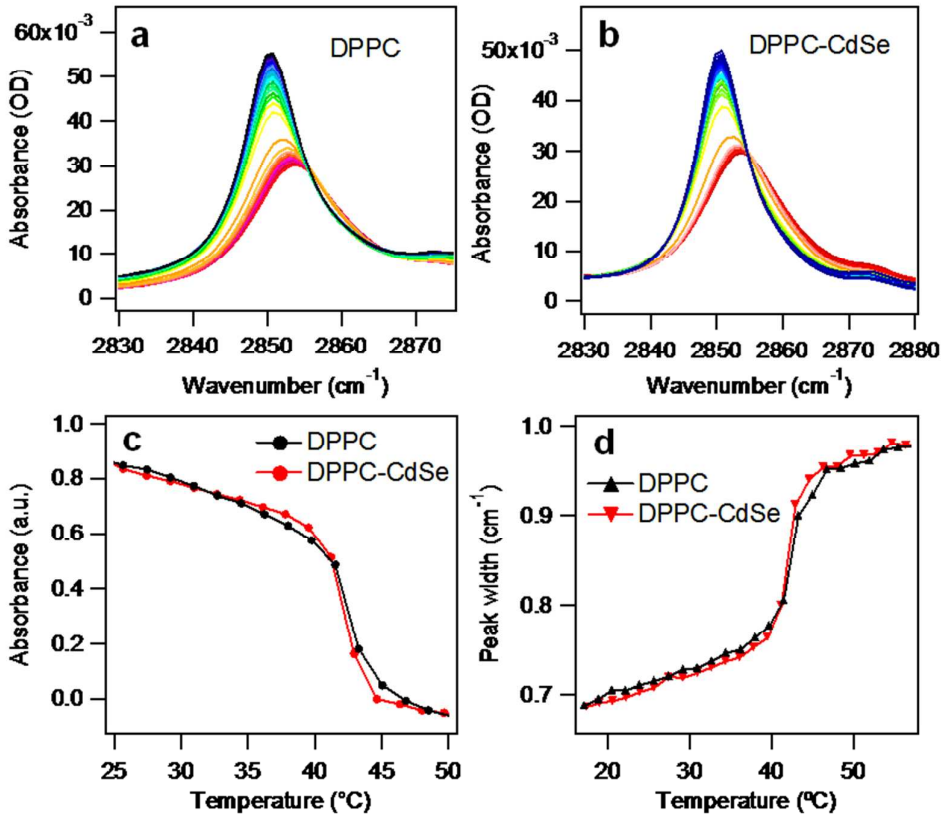


**Figure S4.** Temperature-dependent FTIR spectra of **(a)** DPPC and **(b)** DPPC−CdSe vesicles in the range of 10−65 ºC in ~2 ºC increments. For the FTIR measurements, the 10 mM vesicles were injected into a IR chamber with a 25 μm spacer. **(c)** Thermal phase transition of DPPC and DPPC-CdSe vesicles obtained by plotting the intensity of the $CH_2$ stretch (2851 $cm^{-1}$) versus temperature. **(d)** Temperature-dependent peak width plots for DPPC and DPPC-CdSe vesicles.

Equilibrium temperature-dependent FTIR spectra were recorded on a Varian 3100 FTIR spectrometer equipped with liquid nitrogen cooled mercury cadmium telluride (MCT) detector. The spectra were the result of 256 scans recorded at a resolution of 2 $cm^{-1}$. FTIR spectra on single-component DPPC vesicles and DPPC-CdSe hybrid vesicles are measured as a function of temperature (Figure S11a and S11b). The absorption band at 2851 $cm^{-1}$ is the methylene symmetric stretching mode,[4,5] and is used to probe the lipid phase as a function of temperature. Compared to solid crystalline phases, absorption occurs at distinctly higher wavenumbers in a conformationally disordered liquid phase.[5] The shift to higher frequency in the disordered phase is due to a loss of the mode coupling (inter- and intrachain) that is present in the tightly packed, nearly all-trans conformation in gel phase.[4] Thermal phase transition of DPPC and DPPC-CdSe vesicles obtained by plotting the intensity of the $CH_2$ (2851 $cm^{-1}$) vibrational mode absorption versus temperature yield $T_m$ of 42.0 ± 0.3 ºC for DPPC vesicles and 41.7 ± 0.3 ºC for DPPC-CdSe vesicles (Figure S11c). Figure S11d shows the bandwidth increases during the phase transition. The increase in bandwidth is due to the increased acyl chain disorder, causing an increase in the inhomogeneous broadening, which is consistent with the melting of the ordered gel phase to a disordered fluid or liquid crystalline phase.

**5. Light-induced photo-oxidation of QDs in vesicles.**

**5.1 Photo-oxidation of QDs in vesicles.** L-QD vesicle samples were stored on the bench under room light, while control samples were wrapped in aluminum foil and placed in the dark. The fluorescence of the samples in each environment was monitored using a FluoroMax-3 fluorometer at various points over a 2-month period.

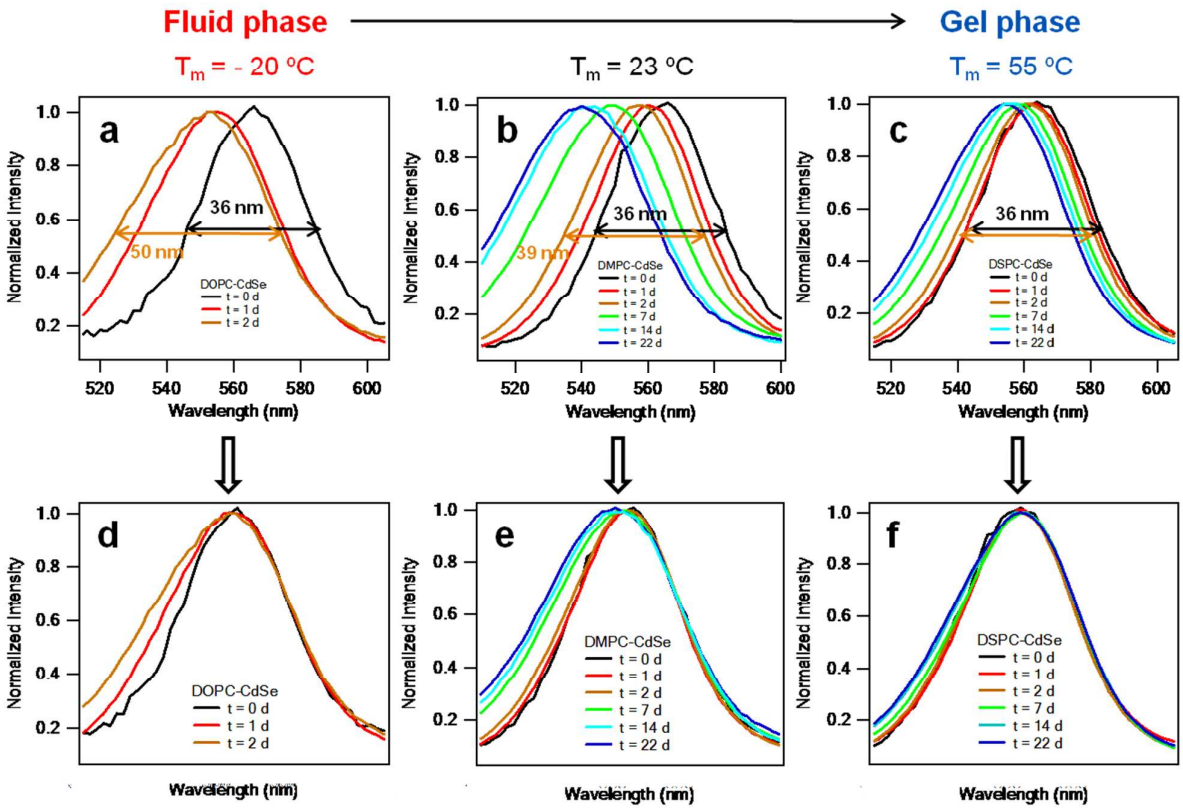


**Figure S5**. Normalized time-dependent PL spectra for **(a)** DOPC-CdSe, **(b)** DMPC-CdSe, and **(c)** DSPC-CdSe vesicles. The PL peaks in **(d)**, **(e)**, and **(f)** were shifted to make the right side overlap with each other to facilitate observing the change in linewidth of the PL spectra.

**5.2 Control experiments of oxidation for 60 days.**

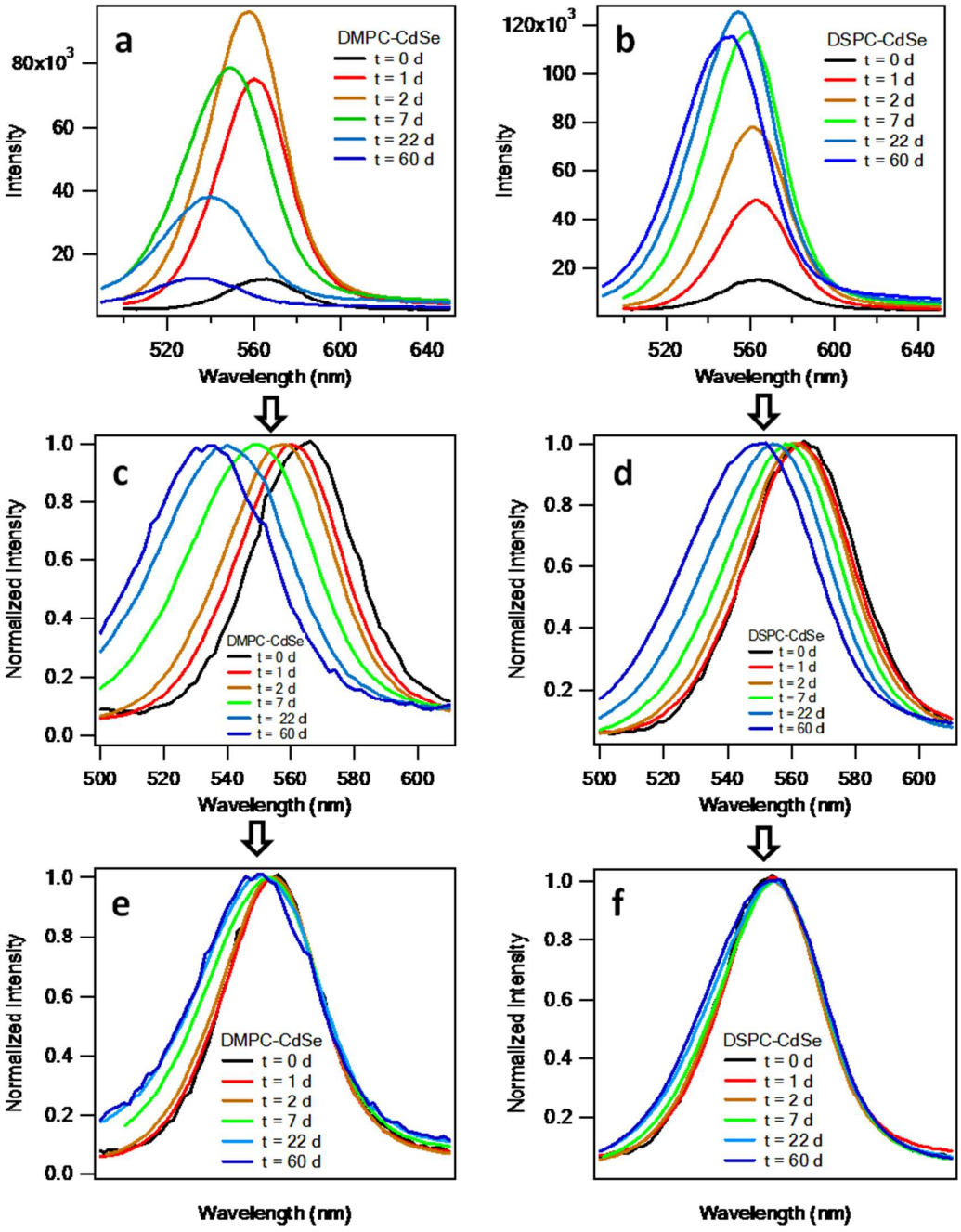


**Figure S6**. Time-dependent PL spectra of CdSe QDs in **(a)** DMPC and **(b)** DSPC vesicles stored under light at room temperature in the time period of 60 days. Normalized PL spectra are shown in **(c)** and **(d)**, respectively. The PL peaks in **(e)** and **(f)** are shifted to make the right side overlap with each other to observe the change in linewidth of the PL spectra.

**5.3 Control experiments of oxidation in dark and under $N_2$.** Note that there were no significant PL spectral changes in peak position, linewidth and intensity observed for identical samples left in the dark over the same period of time (Supplementary Fig. S7), confirming these are light-driven processes. To verify the role of oxygen in driving the PL changes, DOPC encapsulated QDs were stored under a $N_2$ atmosphere and the PL spectra recorded over a period of one month (Supplementary Fig. S8). In this case, QDs remained bright over the entire period, following prior trends of blue shifting and quenching, but with markedly slower rates. Taken together, these results indicate that the PL intensity changes are due to light-induced, and oxygen-mediated photo-oxidation and photo-corrosion processes that are controlled by the organization of the lipid membrane.

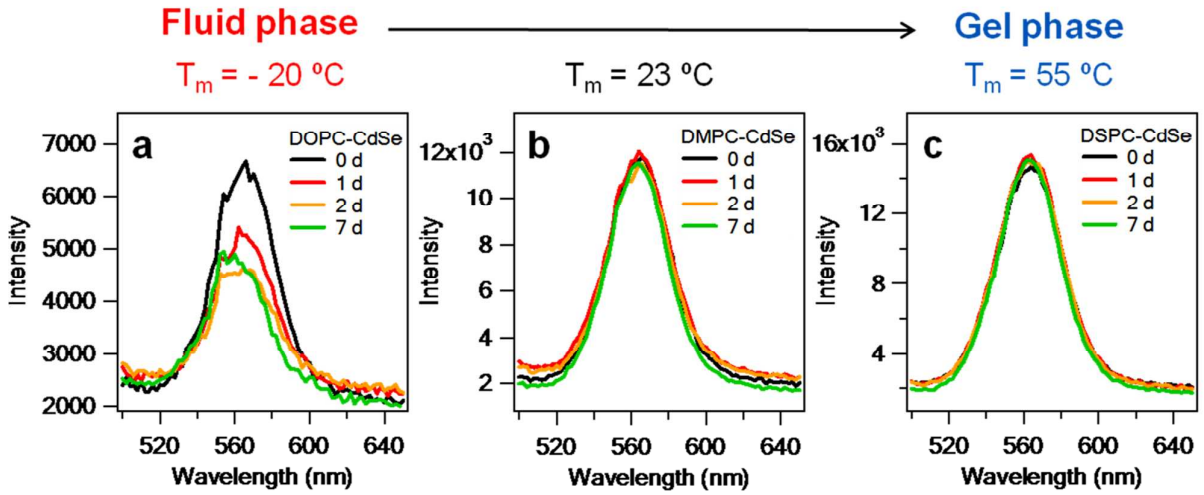


**Figure S7**. PL spectra of CdSe QDs in **(a)** DOPC-CdSe, **(b)** DMPC-CdSe, and **(c)** DSPC vesicles stored in dark room at 4 ºC.

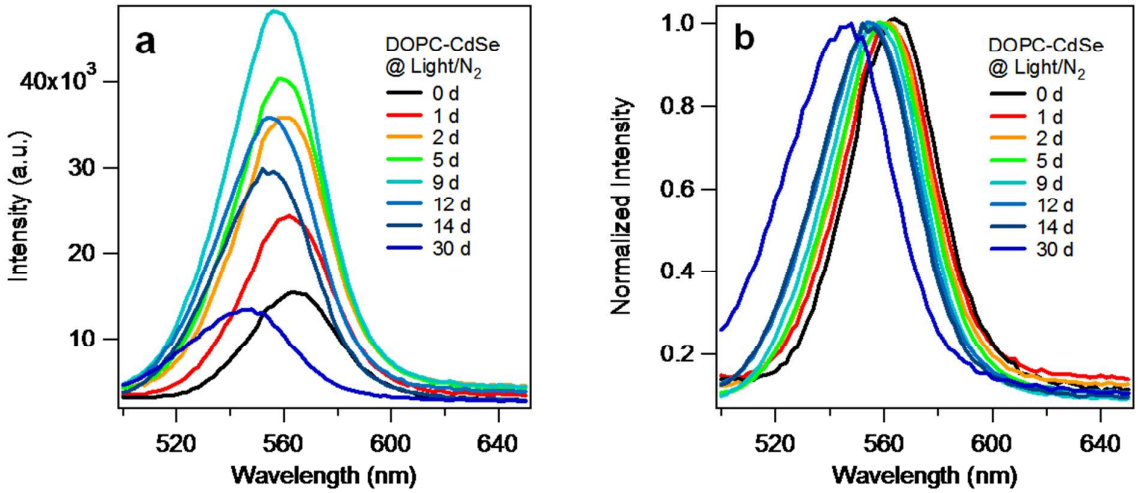


**Figure S8**. **(a)** PL of CdSe QDs in DOPC vesicles stored under light and $N_2$ environment at room temperature. Normalized PL spectra are shown in **(b)**.

**6. Chemical oxidation of CdSe QDs within lipid membrane using $H_2O_2$.**

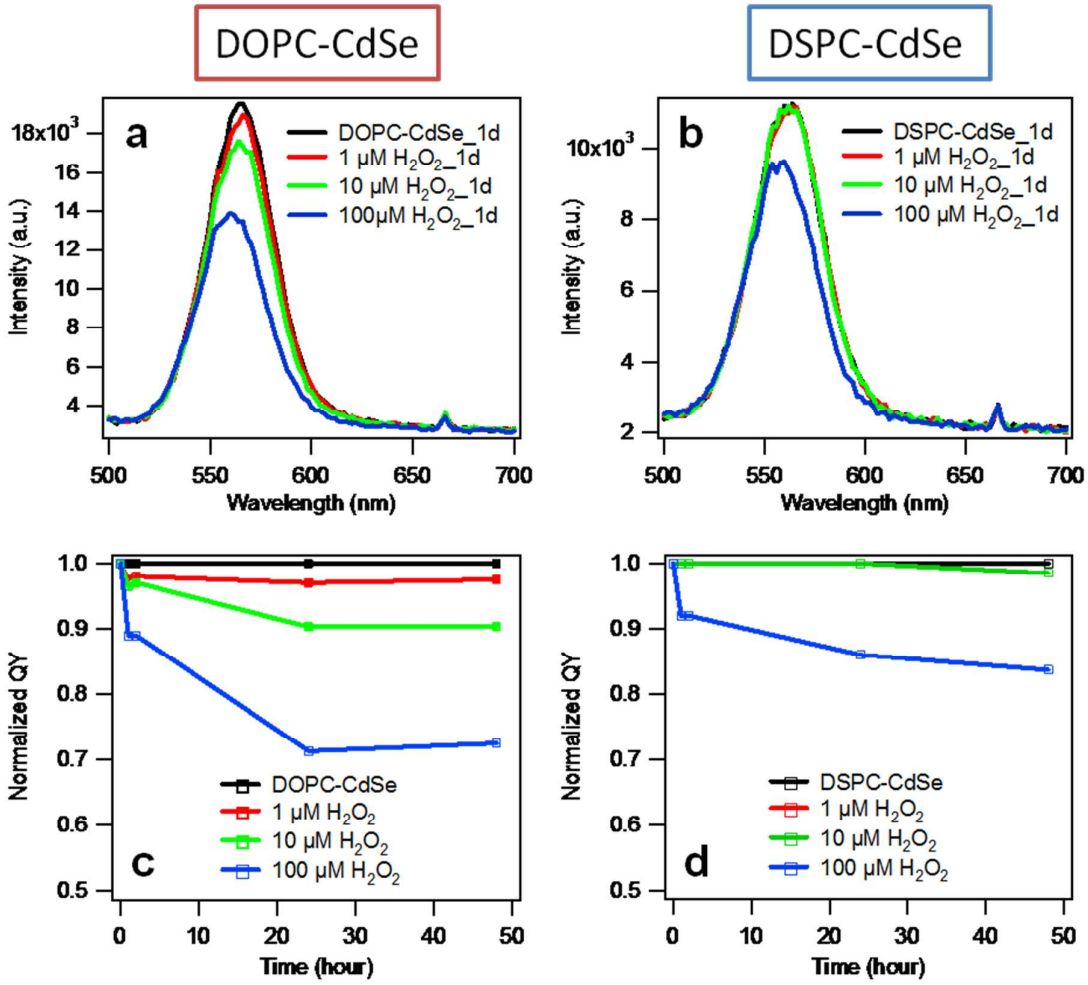


**Figure S9**. PL quenching of CdSe QDs in **(a)** DOPC lipid membrane and **(b)** DSPC lipid membrane by hydrogen peroxide ($H_2O_2$). **(c)** and **(d)** show the time-dependent PL quenching after chemical oxidation of CdSe QDs in DOPC and DSPC vesicles.

Chemical oxidation of 500 nM CdSe QDs by adding $H_2O_2$ at 1 μM, 10 μM, and 100 μM in aqueous solution stored in the dark. From Figure S9, it can be found that:

1) PL quenching at $[H_2O_2] \leq 10$ μM for CdSe in DOPC, but not in DSPC.

2) Higher PL quenching at all $[H_2O_2]$ for CdSe in DOPC than that in DSPC.

3) More significant time-dependent quenching for CdSe in DOPC vesicles, which indicates the larger permeability/diffusion rate of soluble oxides and reactive oxygen species in the lipid membrane.

**7. PL of CdSe QDs encapsulated within DMPC lipid membrane in the gel and fluid phase.** Gel phase DMPC-CdSe vesicles were stored at 4 ºC, while fluid phase samples were maintained at 40 ºC using a water bath. The fluorescence of the samples in each environment was monitored using a FluoroMax-3 fluorometer at various points over a 1-week period.

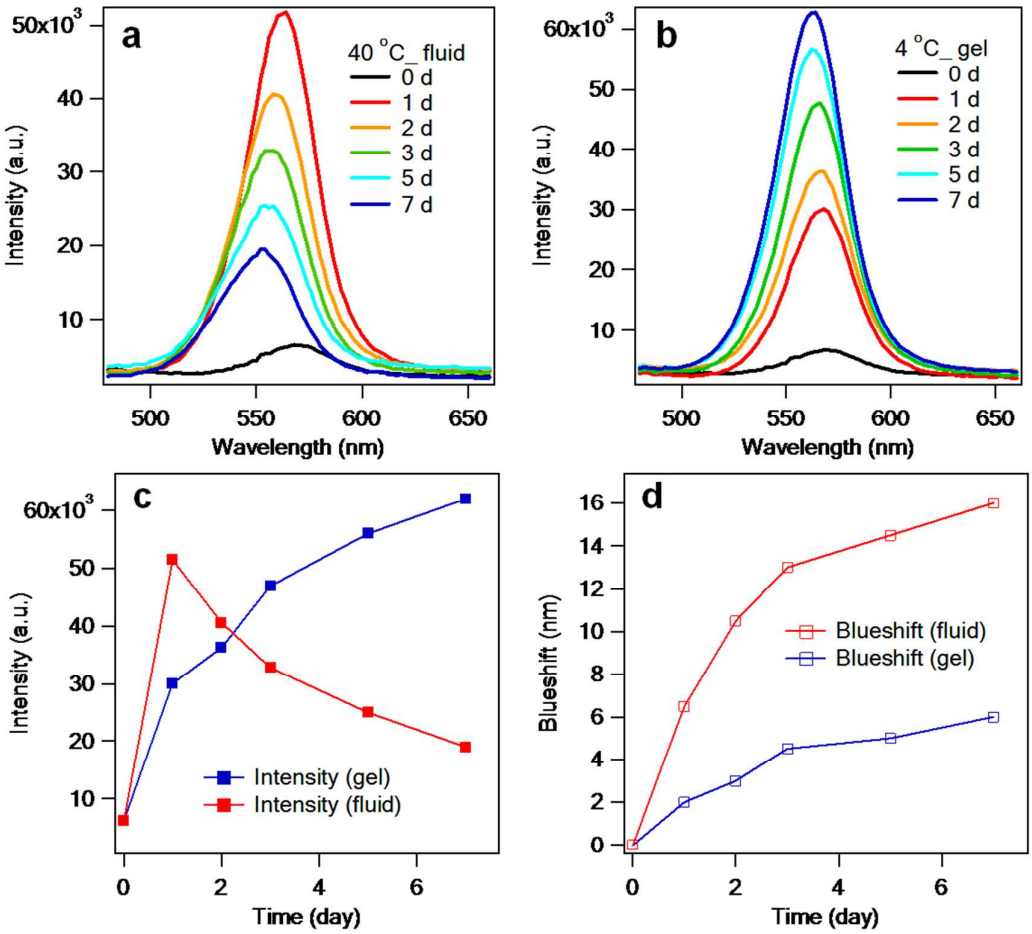


**Figure S10**. **Phase–dependent photostability of CdSe QDs encapsulated within DMPC lipid membranes.** Time-dependent PL spectra of CdSe QDs in DMPC vesicles stored at (**a**) 40 ºC and (**b**) 4 ºC and maintained under the same light source. **c,** Maximum of PL spectra of DMPC-CdSe vesicles as a function of time. **d,** PL blueshifts of DMPC-CdSe vesicles as a function of time.

## 8. Atomistic molecular dynamics (MD) simulation of Lipid-QD assemblies.

**8.1 Simulations methods and force-fields used.** Lipid force-field parameters were based on the Berger forcefield[6] with modifications for DOPC following de Joannis *et al*.[3,7] Cd and Se interactions were via the Rabani force-field.[8] Oleic acid (OA) parameters from Hoopes *et al*. were used,[9] with negative charges on oxygen sites adjusted to give a net charge of zero for each nanoparticle. The water model was SPC.[10] All simulations used Gromacs 4.5.4 with a timestep of 2 fs and temperature maintained at 300 K via Berendsen's method.[11] The Berendsen pressure coupling method was used with semi-isotropic pressure coupling for DOPC and DMPC and with anisotropic pressure coupling for DSPC ($t_p$ = 1.0 ps, 4.5 $e^{-5}$ $bar^{-1}$ compressibility values). Electrostatic interactions were treated via the PME algorithm with a 0.12 grid spacing and cubic interpolation.[12] A cut-off of 1.0 nm was used for the van-der-Waals interactions. The covalent bonds of lipids and those of OA molecule were constrained via the LINCS algorithm.[13] The SETTLE algorithm[14] was utilized in constraining the bonds of water molecules.

**8.2 Oleic acid capped nanocrystal preparation.** The initial coordinates of ~1.2 aspect ratio prolate shaped, Cd rich CdSe quantum dots were generated from sculpting into an wurtzite lattice with constants $a$ = 0.43 nm and $c$ = 7.01 nm[8]. The 100 nanocrystal facet (for a full description of CdSe nanocrystal surface notation see Turner et al.[15]) was left as Cd- and Se- terminated with Se atoms having a single dangling bond. All other nanocrystal surfaces were terminated in Cd atoms. The ~2.6 nm diameter quantum dot has a 462 total number of atoms and a 1.25 Cd:Se stoichiometric ratio. The ~3.4 nm QD has a total of 918 atoms and a 1.21 Cd:Se ratio. The total numbers of ligands capping the ~2.6 nm nanocrystal is 121 OA molecules, a number that results from coordinating each surface Cd atom in a divalent manner. Two ligand capping densities were implemented to cover the ~3.4 nm diameter nanocrystal surface, more specifically 185 OA ligand molecules and 226 OA ligands. The Cd-O bond is implemented as a harmonic bond with an equilibrium inter-separation of 0.24 nm. Increasing the negative partial charges on the oleic acid oxygen atoms counterbalanced the extra charge due to excess Cd surface atoms present in the system.

The ligands were combined with the bare CdSe nanocrystal in the following manner: first, the tail of an oleic acid was stretched out to a linear format preserving the *cis*-kink found at the $C_9$-$C_{10}$ position. The extended ligands were placed with the carboxyl group oxygen atoms at a 0.24 nm distance from a quantum dot surface Cd bonding partner. The ligand shell of fully capped quantum dot was relaxed in vacuum via a 1 ns molecular dynamics (MD) *NVT* ensemble simulation while keeping the nanocrystal structure frozen. At the end of the simulation run, the initial ligand orientation appeared completely isotropic.

**8.3 Combining the capped nanocrystals with lipid bilayers.** In most cases (table S2) a 128 lipid bilayer (prepared as described previously[16,17] was replicated by 2 x 2 x 1 to yield a total 512 lipids assembled into a patch of dimensions 12 nm × 12 nm. A space was created between the leaflets by translating lipid and solvent in the Z-direction by 7 nm. The quantum dot was placed between the two lipid monolayers with the prolate major axis parallel to bilayer normal. The monolayers were next closed to form a bilayer via an applied pressure in the Z-direction, while keeping a fixed $L_x$ x $L_y$ area. The leaflets closed, embedding the quantum dot in 20-50 ps simulation time. The resulting lipid bilayer-QD structures were sampled in ~150 ns NPT molecular dynamics simulations with no restraints.

The initial DSPC bilayer gel configuration was previously realized and characterized in our own group.[18] The production MD simulation conditions differ for the DSPC bilayer in that the Berendsen anisotropic coupling scheme was implemented ($t_p$ = 2.0 ps) that allowed for changes of box/angle dimensions in all three Cartesian directions. For the data analysis purposes, in order to insure Lipid-QD bilayer equilibration, the first 100 ns of MD simulation were excluded for all systems composed of 512 lipids. The frames used during the analysis (> 50 ns in all cases) were sampled across the trajectory at a 15-40 ps resolution.

**Table S2.** Overview of simulated systems

| | Water/Lipid Ratio | QD Size (nm) | Cumulative Simulation Time (ns) |
|---|---|---|---|
| **DOPC** | 54.4 | 2.6 | 150 |
| **DOPC** | 89.6[b] | 3.4 | 150 |
| **DOPC** | 100.1[c] | 3.4 | 150 |
| **DMPC** | 61.1 | 2.6 | 150 |
| **DMPC** | 108.7[b] | 3.4 | 150 |
| **DMPC** | 104.5[c] | 3.4 | 150 |
| **DSPC** | 60.6 | 2.6 | 150 |
| **DSPC** | 60.6[b] | 3.4 | 150 |
| **DSPC** | 103.7[c] | 3.4 | 150 |

b = 226 ligands, c = 185 ligands.

**8.4 Analysis Methods.** Lipid tail orientational time autocorrelation functions were obtained by first finding the unit vector $\mu_i$ directed from carbon 4 to carbon 9 on the *sn*-2 lipid tail of each lipid *i*, then calculating the average autocorrelation function $C_i(t) = \langle \mu_i(\tau) \cdot \mu_i(\tau+t) \rangle$ over the trajectory segment from $\tau$ = 100 to $\tau$ = 150 ns for *t* up to 25 ns. The averages of $C_i(t)$ were taken over lipids *i* classified as either bulk-like (far from the QD) or perturbed (near to the QD). Lipids were classified as near or far from the QD based on their radial distance in the XY plane from the QD center-of-mass. The cut-off radius was determined for each structure as the distance at which the lipid bilayer recovered its unperturbed thickness. In the case of DSPC, a subset of lipids within the cut-off radius had gel-like properties; in these, the orientational autocorrelation function persisted above 0.92 over the 25 ns analysis range. These 20-30% of lipids were excluded from the average plotted in Fig. 4.

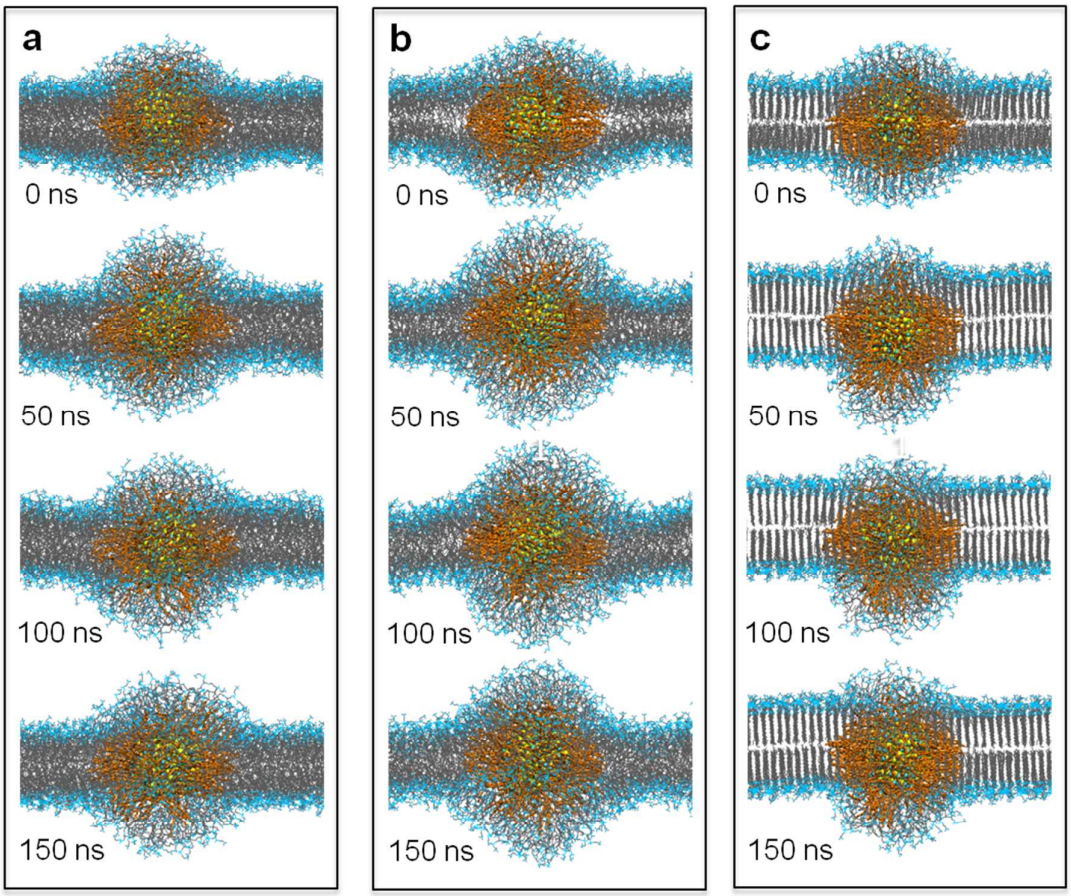


**Figure S11**. Snapshots of atomistic MD simulation of 3.4 nm CdSe QD in fluid phase DOPC (185 OA) (**a**), DMPC (226 OA) (**b**), and gel phase DSPC (226 OA) lipid membranes.

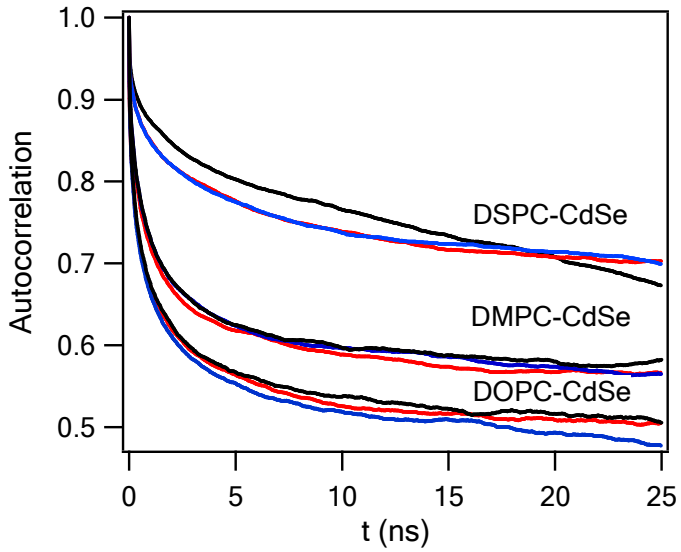


**Figure S12.** Autocorrelation function decay variability with size of nanocrystal and ligand density from lipids that interact with QD passivating ligands: 2.6 nm QD/121 OA (black line), 3.4 nm QD/226 OA (red line), and 3.4 nm QD/185 OA (blue line).

**9. Selective ligand exchange data for L-QD vesicles.**

**9.1 Selective ligand exchange with SH-PEG for QDs.**

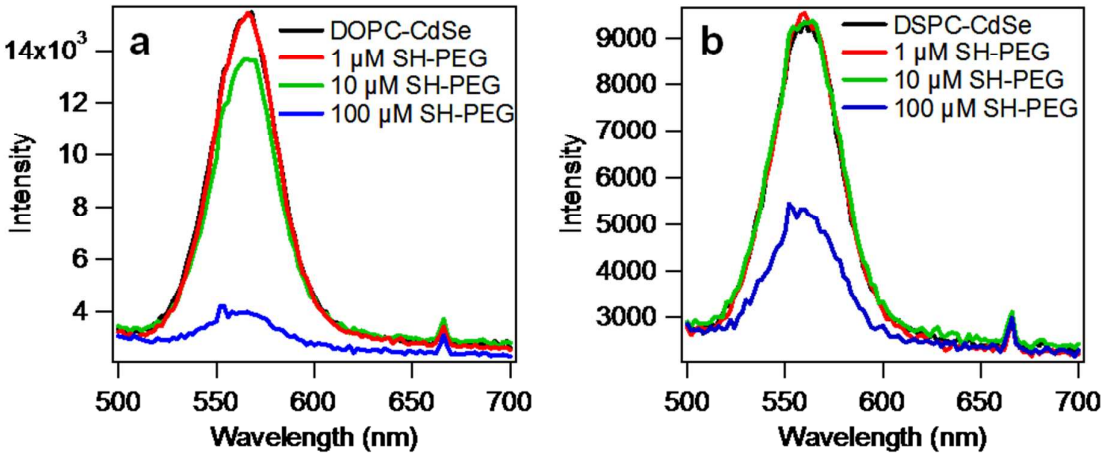


**Figure S13.** PL spectra of Lipid-QD vesicle incubated with SH-$(CH_2CH_2O)_8CH_3$ ligand for one day.

**9.2 Synthesis of SH-PEG-Cy5 ligand and ligand exchange for QD in L-QD vesicles.** 0.26 mg of amine-$PEG_{82}$-thiol was mixed with 100 μg Cy5-NHS ester in 7.7μL DMF with 0.2 μL TEA. The reaction was carried out for 12 h and followed by size exclusion chromatography with a 4000 MW cutoff (P4 gel). The purity of the final product was confirmed by HPLC to be 98%. 10 μM SH-PEG-A488 solutions were then mixed with L-QD vesicles for ligand exchange. The selective ligand exchange for CdSe QDs using fluid phase DOPC lipid template is further confirmed by fluorescence measurements using a fluorescent dye (Cy5) conjugated to thiolated PEG ligand. SH-$(CH_2CH_2O)_{82}$-Cy5 ligand (10 μM) was added in 200 μL lipid-QD aqueous solution with 500 nM QD concentration in a 96 well plate. After sample incubation in the dark for more than 2 hours, excess ligand was removed via rinsing with DI water 5 times to reduce the background signal from free ligand in the solution.

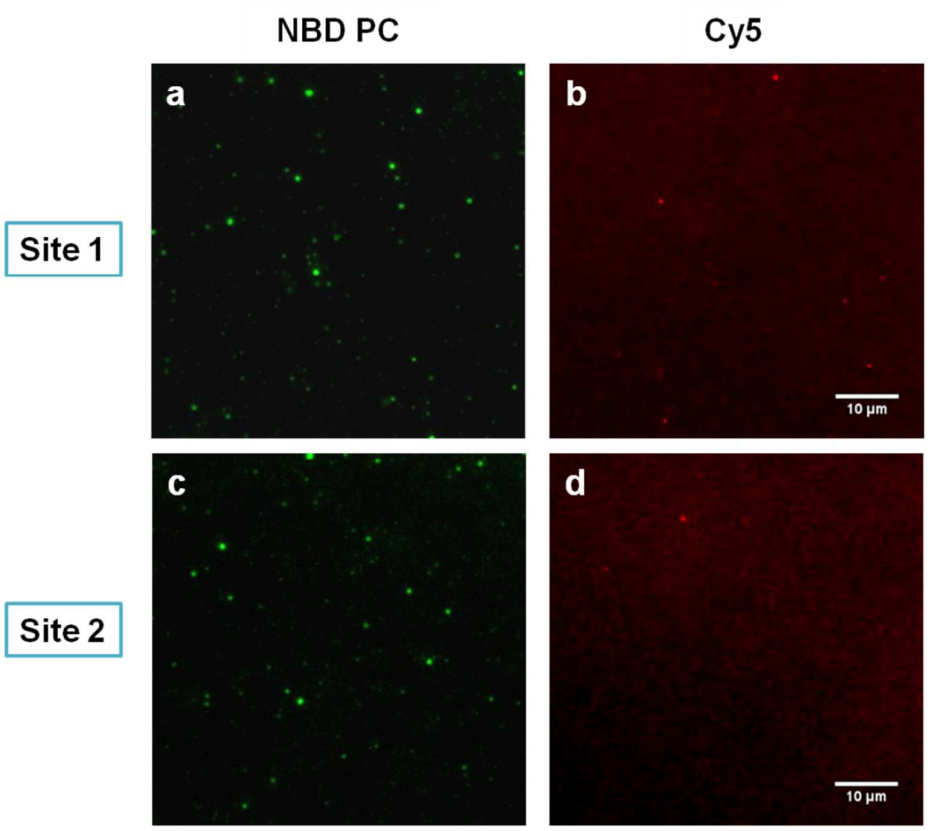


**Figure S14**. Control experiment where NBD-PC doped DOPC vesicles were exposured to 10 µM SH-PEG$_{82}$-Cy5 ligands for 10 hrs. **(a)** and **(c)** show fluorescence from the NBD PC channel. **(b)** and **(d)** shows fluorescence of the Cy5 channel in the same region as in **(a)** and **(c)**. Compared with fluorescence from NBD-PC doped vesicles, only a few particles were observed in the Cy5 channel after the glass chamber was rinsed with water. Furthermore, no co-localization of NBD-PC doped vesicles and Cy5 ligand was observed indicating no binding occurred between DOPC vesicles lacking QDs and SH-PEG$_{82}$-Cy5 ligands.

**9.3 Stoichiometry of ligand binding after ligand exchange.** Given that ligand exchange occurs exclusively for QDs in fluid membranes when incubated at 10 μM, we next wanted to determine the average number ligands per QD. UV-vis absorption spectroscopy was used to determine the molar ratio of Cy5 to QDs in CdSe-DOPC samples following ligand exchange with 10 μM SH-$PEG_{82}$-Cy5, and repeated cycles of centrifugation and washing. The resulting DOPC-CdSe material was finally suspended in chloroform to reduce scattering and improve the precision of the absorption measurement.

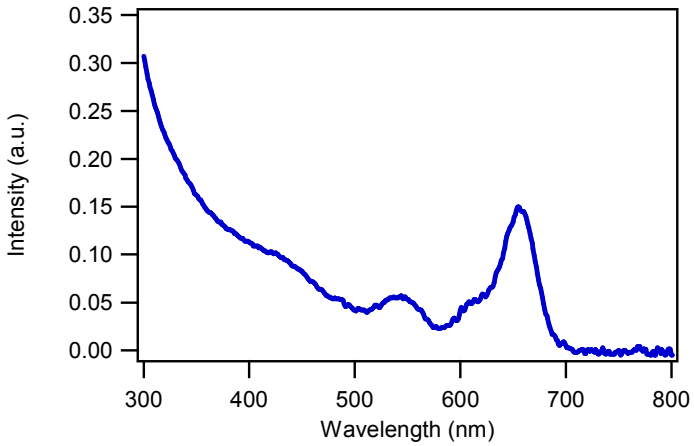


**Figure S15.** Absorption spectrum of CdSe-PEG-Cy5 after incubating CdSe-DOPC vesicles with SH-$PEG_{82}$-Cy5 (10 μM) for 10 hrs. After ligand exchange, the CdSe-DOPC vesicles were separated from solution via centrifugation, then re-dissolved in chloroform.

This allowed us to determine the stoichiometry between Cy5 and QDs as approximately *two* to *three* ligands per particle, suggesting that only a few sites are available for ligand exchange under these conditions.

## 10. Generating QD-DNA-AuNP hybrid structures in lipid vesicles..

**10.1 Synthesis of AuNPs.** Citrate-stabilized AuNPs (14.8 ± 0.8 nm) were prepared using published procedures.[19] Briefly, a 500 mL solution of 1 mM hydrogen tetrachloroaurate (III) trihydrate was brought to a vigorous boil, and once boiling, 50 mL of a 38.8 mM sodium citrate tribasic dihydrate solution was added and allowed to reflux for 15 min. The reaction mixture was filtered using a 0.45 μm acetate filter, producing monodisperse AuNPs. The extinction spectrum of the AuNPs was determined using UV-vis spectrometry, and particle size was verified using transmission electron microscopy (TEM).[20,21]

**10.2 Synthesis of SH-DNA modified Au NPs.** Disulfide-modified oligonucleotides at the 3' terminus were purchased from Integrated DNA Technologies (IDT). The disulfide was reduced to a free thiol by incubating 35 nmols of lyophilized oligonucleotide with 700 μL of disulfide cleavage buffer (0.1 M dithiothreitol (DTT), 170 mM phosphate buffer at pH 8.0) for 3 h at room temperature. The reduced oligonucleotides were purified using a NAP-25 column (GE Healthcare, Piscataway, NJ) with Nanopure water as the eluent.

AuNPs were functionalized with 3' alkanethiol oligonucleotides following a modified literature protocol.[19] Freshly cleaved oligonucleotides were added to citrate stabilized gold nanoparticles in Nanopure water. Next, 10X phosphate buffer and 100X sodium dodecyl sulfate (SDS) stock solutions were added to the gold nanoparticle solution to bring the final concentration to 0.01M and 0.01% respectively. The oligonucleotide/gold nanoparticle solution was allowed to incubate at room temperature for 20 min. The concentration of NaCl was increased to 0.7 M using 2 M NaCl, 0.01 M PBS stock solution through 8 additions at increments of 0.05 M NaCl for the first two additions and 0.1 M for all subsequent additions. The particles were immediately sonicated for 10 s after each salt addition and incubated for 20 minutes to maximize DNA packing. The fully salted particles were then incubated overnight, in the dark and at room temperature. The following day, the particles were centrifuged four times at 13,500 rpm, reconstituted in Nanopure water each time, and stored at 4 ºC for future use.

**10.3 Hybrid Au-DNA-QD constructs.**

**Scheme S1.** Au-DNA-QD structure linked by double stranded DNA.

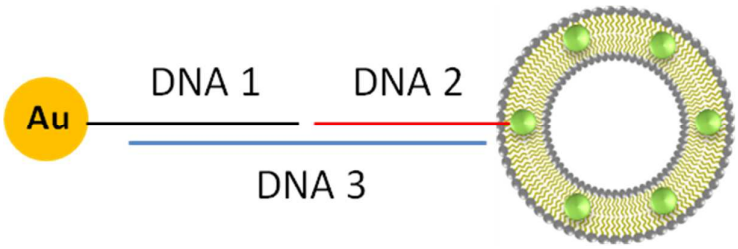


**DNA 1:** 5'-GCA CCC AGG CTA GCT ACA ACG ACT CTC TC T10-SH-3'

**DNA 2:** 5'-SH- GCC TAT GAA TGA GCT TCA GTG -3'

**DNA 3:** 5'- GAG AGA GTC GTT GTA GCT AGC CTG GGT GCC ACT GAA GCT CAT TC -3'

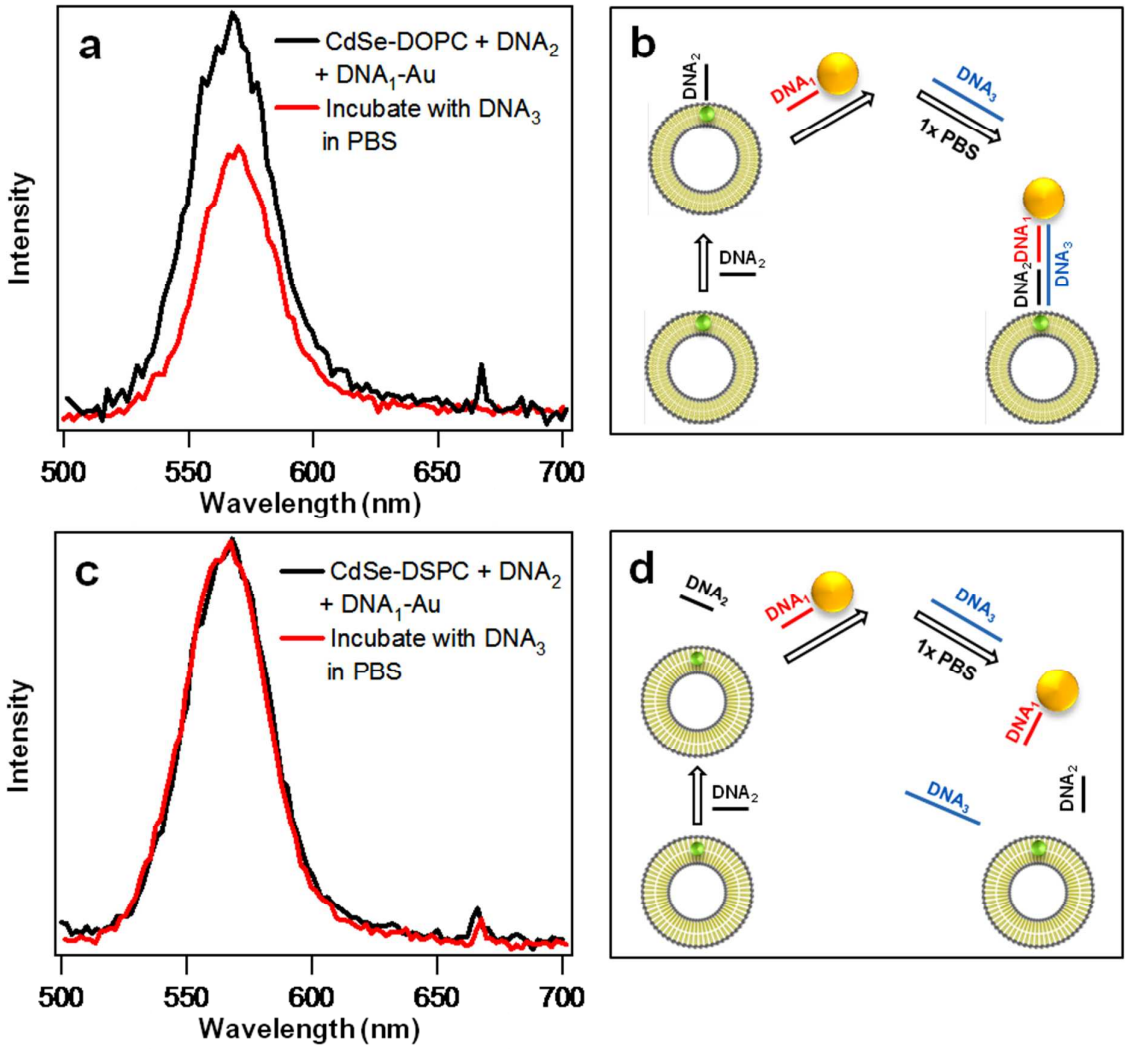


**Figure S16.** PL spectra of QD-DOPC (**a** and **b**) and QD-DSPC (**c** and **d**) vesicles incubated with thiolated $DNA_2$ and 10 μM $DNA_1$-modified AuNPs (black line in **a** and **c**). These spectra (black line in **a** and **c**) represent mixtures of L-QD vesicles and AuNPs that are not hybridized, and were used as a reference to account for the filter effect of AuNP absorption at 520 nm. The PL spectra shown in red (**a** and **c**) were collected after the addition and overnight hybridization of $DNA_3$ that is partly complementary to both $DNA_1$ and $DNA_2$. The ~30% quenching of the QD emission when encapsulated in DOPC confirms the close proximity (~1-20 nm) and assembly of AuNP to the QD surface.

**11. Caption for Supplementary Video 1**: Animation showing 150 ns molecular dynamics trajectories performed on 2.6 nm CdSe QD embedded in DOPC (upper) and DSPC (lower) bilayers, with the QD and oleic acid ligands highlighted and solvent omitted. Temperature was set to 300 K.

**Supplementary References:**


(1) Li, J. J.; Wang, Y. A.; Guo, W.; Keay, J. C.; Mishima, T. D.; Johnson, M. B.; Peng, X. *J. Am. Chem. Soc.* **2003**, *125*, 12567-12575.

(2) Peng, Z. A.; Peng, X. *J. Am. Chem. Soc.* **2001**, *123*, 183-184.

(3) Yu, W. W.; Qu, L.; Guo, W.; Peng, X. *Chem. Mater.* **2003**, *15*, 2854-2860.

(4) Nagarajan, S.; Schuler, E. E.; Ma, K.; Kindt, J. T.; Dyer, R. B. *J Phys Chem B* **2012**, *116*, 13749-13756.

(5) Forstner, M. B.; Yee, C. K.; Parikh, A. N.; Groves, J. T. *J. Am. Chem. Soc.* **2006**, *128*, 15221-15227.

(6) Berger, O.; Edholm, O.; Jähnig, F. *Biophys. J.* **1997**, *72*, 2002-2013.

(7) de Joannis, J.; Coppock, P. S.; Yin, F. C.; Mori, M.; Zamorano, A.; Kindt, J. T. *J. Am. Chem. Soc.* **2011**, *133*, 3625-3634.

(8) Rabani, E. *J. Chem. Phys.* **2001**, *115*, 1493.

(9) Hoopes, M. I.; Noro, M. G.; Longo, M. L.; Faller, R. *J. Phys. Chem. B* **2011**, *115*, 3164-3171.

(10) Berendsen, H. J. C.; Postma, J. P. M.; van Gunsteren, W. F.; Hermans, J. In *Intermolecular Forces*; Pullman, B., Ed.; D. Reidel: Dordrecht, 1981.

(11) Berendsen, H. J. C.; Postma, J. P. M.; DiNola, A.; Haak, J. R. *J. Chem. Phys.* **1984**, *81*, 3684-3690.

(12) Essman, U.; Perera, L.; Berkowitz, M. L.; Darden, T.; Lee, H.; Pedersen, L. G. *J. Chem. Phys.* **1995**, *103*, 8577-8592.

(13) Hess, B.; Bekker, H.; Berendsen, H. J. C.; Fraaije, J. *J. Comput. Chem* **1997**, *18*, 1463-1472.

(14) Miyamoto, S.; Kollman, P. A. *J. Comput. Chem.* **1992**, *13*, 952-962.

(15) Taylor, J.; Kippeny, T.; Rosenthal, S. J. *Journal of Cluster Science* **2001**, *12*, 571.

(16) West, A.; Ma, K.; Chung, J. L.; Kindt, J. T. *J. Phys. Chem. A* **2013**, *117*, 7114-7123.

(17) Coppock, P. S.; Kindt, J. T. *Langmuir* **2008**, *25*, 352-359.

(18) Coppock, P. S.; Kindt, J. T. *Langmuir* **2009**, *25*, 352-259.

(19) Hill, H. D.; Mirkin, C. A. *Nat Protoc* **2006**, *1*, 324-336.

(20) Liu, Y.; Yehl, K.; Narui, Y.; Salaita, K. *J. Am. Chem. Soc.* **2013**, *135*, 5320-5323.

(21) Yehl, K.; Joshi, J. P.; Greene, B. L.; Dyer, R. B.; Nahta, R.; Salaita, K. *ACS Nano* **2012**, *6*, 9150-9157.